Computer-Aided Civil and Infrastructure Engineering **21** (2006) 395–410

Segmentation of Pipe Images for Crack Detection in Buried Sewers

Shivprakash Iyer & Sunil K. Sinha*

Department of Civil and Environmental Engineering, The Pennsylvania State University, University Park, PA 16802, USA

Abstract: *Assessing the condition of underground pipelines such as water lines, sewer pipes, and telecommunication conduits in an automated and reliable manner is vital to the safety and maintenance of buried public infrastructure. To fully automate condition assessment, it is necessary to develop robust data analysis and interpretation systems for defects in buried pipes. This article presents the development of an automated data analysis system for detecting defects in sanitary sewer pipelines. We propose a three-step method to identify and extract cracks from contrast enhanced pipe images. This method is based on mathematical morphology and curvature evaluation that detects crack-like patterns in a noisy pipe camera scanned image. As cracks are the most common defects in pipes and are indicative of the residual structural strength of the pipe, they are the focus of this study. This article discusses its implementation on 225 pipe images taken from different cities in North America and shows that the system performs very well under a variety of pipe conditions.*

1 INTRODUCTION

The public infrastructure is the lifeblood of every community. The United States has an estimated $20 trillion investment in civil infrastructure systems. But many of these systems are eroding due to aging, excessive demand, misuse, exposure, mismanagement, and neglect (Chae and Abraham, 2001). Communal sewer networks are often one of the biggest infrastructures of an industrialized country, accounting for around 3,200 miles of sewers per million citizens (Duran et al., 2002). According to the U.S. Environmental Protection Agency and claims by other sources, there are approximately 1 million miles of sewers in the United States (Chae and Abraham, 2001). It has been estimated that upward to 40% of the United States' underground infrastructure will have failed or will be on the brink of failure within 20 years, unless efforts are initiated to renew it (Technical Report (WIN), 2001, 2002). But system renewal requires adequate funding. According to an April 2000 report by the Water Infrastructure Network (WIN) Agency, "America's water and wastewater systems face an estimated funding gap of $23 billion a year between current investments in infrastructure and the investments that will be needed annually over the next 20 years to replace aging and failing pipes and meet mandates of the Clean Water Act and Safe Drinking Water Act" (Technical Report (WIN), 2001). This necessitates the need to monitor, detect and prevent any unforeseen failures in the working of these underground pipelines that are complex in nature.

Research in the area of highways has matured and has become the basis for studies in sewer systems. The understanding of sewer deterioration mechanisms helps asset managers in developing deterioration models to estimate whether sewers have deteriorated to the point of collapse (Iseley, 1999). Various imaging technologies have emerged over the years and have been applied to inspect the state of deterioration (Haas et al., 1998; Gokhale et al., 1997). The state of deterioration in a sewer pipe is estimated based on the presence of surface defects like cracks, holes, fissures, spalling of surface material, and so on. Among all these defects, cracks are of interest to municipal engineers because detecting and monitoring them at an early stage will help prevent sudden failures and aid authorities in taking critical decisions pertaining to maintenance and rehabilitation (M& R) of these infrastructures. Research in monitoring

*To whom correspondence should be addressed. E-mail: *sunil@engr.psu.edu.*

methods for crack detection in pavement surfaces have led to innovative ways of automating and detecting structural cracks in pipe surfaces (Gharpuray and Haas, 1993). Most municipal pipeline systems in North America are inspected visually by mobile closed-circuit television (CCTV) systems to access the structural integrity of underground pipes (Gokhale et al., 1997). The video images are normally examined visually and classified into grades according to the extent of damage (size of cracks, holes) against the documented criteria. Although the human eye is extremely effective at recognition and classification, it is unreasonable to assume its suitability for assessing pipe defects in thousand of miles of pipeline images due to fatigue and subjectivity. This motivates the development of an automated pipe inspection system that can access pipe conditions by detecting defects like cracks to ensure accuracy, efficiency, and economy in the condition assessment phase. In a camera based inspection system, image preprocessing and segmentation is the initial stage for any recognition process, where by the acquired image is partitioned into meaningful regions or segments. Therefore, it is very important to understand the basic image and to model its features to accurately extract features of interest. As the image obtained by scanning a buried sewer pipe is very complex in terms of its features, it is important to preprocess the image before attempting to apply segmentation and feature extraction algorithms.

This article proposes an automated image analysis and defect detection methodology as an intermediate step toward complete automation of data acquisition, analysis, and eventually condition rating based on feature classification. In the following sections, a new approach to preprocessing image data using an improved contrast-enhancement method and final crack detection using *mathematical morphology* and a *curvature evaluation* based algorithm derived from digital imaging principles are presented.

2 AUTOMATED PIPE INSPECTION

Internal inspection of pipelines are done by detection systems ranging from simple visual inspection to complex imaging systems. Some promising nondestructive diagnostic methods using infrared thermography, ground penetrating radar and pulse-echo have been used for condition assessment of sewer pipelines around the world. However, there is a common consensus that these inspection methods do not characterize the complete picture of the condition of sewers due to their dependability on unimodal data collection (Chae and Abraham, 2001). Although, there are various destructive and nondestructive inspection methods, we will limit our discussion to the two most advanced and applicable techniques, namely, the CCTV inspection system and the sewer scanner and evaluation technology (SSET). These methods consist of a wheeled remotely operated video camera and a lighting system. The camera platform is connected via a physical multicore cable to a remote station situated over ground. The cable is used for transmitting power supply and data, determining the distance traveled, and also allowing to manually pull the platform to safety in case of malfunction. CCTV is a cost-effective method to assure proper installation, object location, infiltration, or defect in the pipeline. Detailed descriptions on different commercial platforms and CCTV cameras can be found in Morici (1997). Factors like experience of the operator, skill level, concentration, and reliability of the picture quality significantly influence the accuracy of defect or failure diagnosis. Hence, this method is suitable only for detecting gross defects that can easily be picked up in a forward vision (FV) view of the CCTV camera (Chae and Abraham, 2001).

SSET is an innovative Japanese technology designed to nondestructively survey and inspect the interior condition of sewer pipelines. SSET uses optical scanning and gyroscopic technologies to produce a detailed digital image and provides an alternative to commonly practiced CCTV inspection methods. Figure 1 shows a SSET system with inspection probe and typical unwrapped images. Various defects in sewer pipes are generally shown accurately, with the image resolution being adequate to clearly indicate their type and size in most cases. At its current stage of development, SSET provides the basis for future sewer management tools that will become

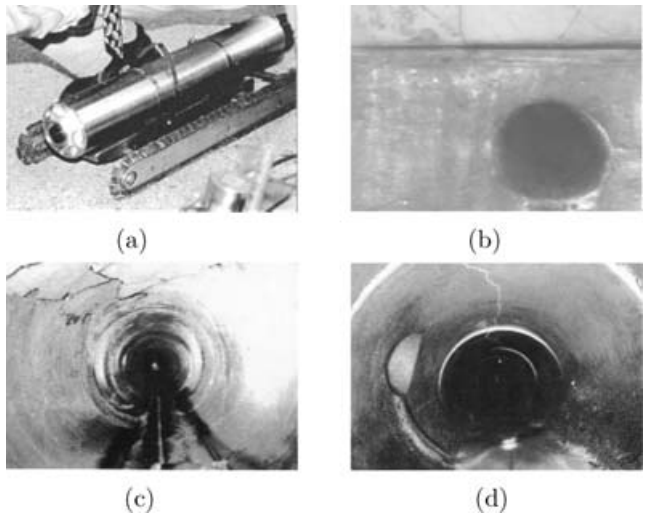

Fig. 1. (a) SSET inspection probe, (b) typical unwrapped digital image of a scanned pipe, (c) and (d) forward vision (FV) image from CCTV camera (Trenchless Technology Magazine, 1999).

much more powerful as automated defect recognition software is developed (Technical Report (SSET), 2001). The SSET and CCTV provide images that are primarily in color although the SSET images are of the pipe surface scanned circumferentially as against the CCTV images that provide a forward vision of the pipe from inside. Another advantage of SSET is that it travels continuously from one manhole section to another as it collects the gyroscope data whereas the operator needs to stop the operation when the CCTV system encounters a pipe defect to record it.

The methodology developed by the North America Association of Pipeline Inspectors (NAAPI) is used to quantify the sewer main condition based on video (or surface scan image) feeds. The NAAPI methodology consists of assigning a score to the cracks based on certain set criteria as discussed in the *NAAPI Manual of Sewer Condition Classification*. The higher the NAAPI score, the greater the seriousness of the cracks and higher the probability of a failure. Although pipe scan data are acquired using automated technologies like the CCTV and SSET, crack detection and classification is still done by manual operators in the field or off-line which brings in the issue of subjectivity, fatigue and life-cycle cost over extended periods. Therefore, reliable automated detection and classification systems that incorporate the NAAPI scoring system without the need for a human operator, are highly desirable under such conditions to compensate for the subjective interpretation of pipe scan images. This is a complex task because of the continuously changing pipe background scenarios, illumination, and crack patterns.

3 LITERATURE REVIEW

Most of the literature concerning the detection of defects (like cracks) in civil structures deals with the analysis of pavement and concrete/steel distress that are not directly applicable to underground pipe inspection (Cheng and Miyogim, 1998; Chae and Abraham, 2001; Gokhale et al., 1997). In analyzing underground pipe scanned image data, it is imperative to consider complications due to inherent noise in the scanning process, irregularly shaped cracks, as well as the wide range of pipe background patterns. In the past two decades, many approaches have been developed to deal with the detection of linear features on retinal, satellite and most recently, underground pipe images (Merlet and Zerubia, 1996; Hellwich et al., 1992; Fieguth and Sinha, 1999; Sharpe et al., 1995; Chae and Abraham, 2001; Gokhale et al., 1997). Most of them combine a local criterion evaluating the radiometry on some small neighborhood surrounding a target pixel to discriminate lines from the background and a global criterion introducing some large scale a priori knowledge about the structures (e.g., cracks) to be detected.

The techniques used for pavement distress detection in scanned images are based on conventional edge or line detectors with respect to local criterion (Mohajeri and Manning, 1991; Walker and Harris, 1991). These methods evaluate differences of averages, thus indicating noisy results and inconsistent false-alarm rates. This necessitates the introduction of global constraints owing to insufficiency of local criterion in line and edge detection. As cracks in underground scanned pipe images resemble undulating curves with a generally constant width, Hough transform-based approaches have also been tested for the detection of parametric curves, such as straight lines or circles (Skingley and Rye, 1987). Tracking methods and energy minimization methods, such as snakes, have been used to track roads in satellite images and heart walls in live feeds from medical ultrasound angiographies (Geman and Jedynak 1996; Kass et al., 1998). These tracking methods find a minimum cost path in a graph by using some heuristics like an entropy criterion. Statistical methods such as those that employ a Bayesian framework complemented by cross-correlation detectors have been used to detect cracks to a reasonable accuracy level (Fieguth and Sinha 1999; Sinha et al., 1999, 2000; Sinha and Knight, 2001; Sinha and Fieguth, 2001). However, their results were noisy with high false-alarm rates when the image had a dark background with multiple cracks in a tree-like geometry. Chae and Abraham (2001) developed neuro-fuzzy approaches for detecting and classifying pipe defects. They used a histogram-based contrast enhancement scheme to convert RGB format digital color images to grayscale images as a preprocessing step before applying a gradient-based edge detection scheme to segment pipe defect features. Morphology-based filtering coupled with cross-curvature evaluation has not been used to detect cracks and remains an unexplored frontier. We will show that the application of some carefully selected morphological filters leads to a simplified image whose cross-curvature evaluation can be easily done for segmenting crack pixels from the image.

4 AUTOMATED CRACK DETECTION

Two aspects are important from the automation of crack detection viewpoint; a contrast enhancement scheme and an effective crack segmentation methodology. In this section, we present a brief discussion on contrast enhancement, mathematical morphology, and curvature evaluation before attempting to describe our algorithm for automated crack detection consisting of certain

carefully selected morphological filters. Curvature evaluation of the resulting image from the morphological segmentation phase yields a binary crack map that can be used to measure the crack and determine pipe criticality levels.

4.1 Contrast enhancement

The use of digital image data for a spatial database requires several preprocessing procedures. These procedures include, but are not limited to: geometric correction, image enhancement, and feature selection. The goal of digital image preprocessing is to increase both the accuracy and the interpretability of the digital data during the image processing phase (Gonzalez and Woods, 2002). The aim of preprocessing in underground pipeline images is an improvement of the image data that suppresses unwanted distortions in background or enhances some image features (like cracks in this study) important for further processing. This will allow for accurate spatial assessments and measurements of crack features from the SSET or CCTV imagery.

The presence of various features in an acquired image (see Figure 2) poses considerable challenge in detecting the desired structural failure patterns such as cracks, fissures, and so on. As seen in Figure 2, various features exist that make it complex for a recognition system to classify the desired patterns. Hence, this necessitates the application of low-level methods of image preprocessing to enhance the contrast between various features in the acquired image. The principal objective of image enhancement techniques is to process an image so that the result is more suitable than the original image for specific application. "Specific" in our case applies to enhancing contrast between the background of pipe and desired crack features. Crack features are deeper than the pipe surface. This causes the deep regions to produce color

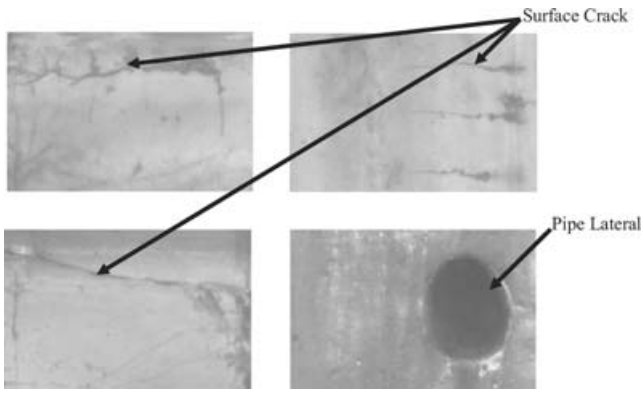

Fig. 2. Sample images from SSET showing different crack patterns, pipe lateral and varying illumination level.

pixels with a characteristic intensity compared to the rest of the image. We will briefly discuss two methods of contrast enhancement adopted for this study in Section 4.4.1.

4.2 Mathematical morphology

The techniques of mathematical morphology are based on set-theoretic concepts, on the nonlinear superposition of the signal, and on a class of nonlinear systems that we call morphological systems. This section is a brief review of fundamental definitions of morphological operators considered in this study. Advanced information on mathematical morphology can be found in Serra (1982) and Maragos and Schafer (1990).

For our reference, we will define a two-dimensional (2D) grayscale image having an intensity range of $[I_{\min}, I_{\max}]$ as a functional F: $R^2 \rightarrow [I_{\min}, I_{\max}]$, and a 2D structural element as a functional B: $R^2 \rightarrow \boldsymbol{B}$ where $\boldsymbol{B}$ is the set of the neighborhoods of the origin. We consider structuring elements invariant by translation that are identified with a subset of R^2 and are referred to as linear structuring elements when this subset is a line segment. Basic morphological operators with respect to the structuring element B, a scaling factor e, image F, and a processing point $P_0 \in R^2$ can be defined as:

$$\text{erosion:} \quad \epsilon_B^e(F)(P_0) = \text{MIN}_{P \in P_0 + e \cdot B(P_0)}(F(P)); \quad (1)$$

$$\text{dilation:} \quad \delta_B^e(F)(P_0) = \text{MAX}_{P \in P_0 + e \cdot B(P_0)}(F(P)); \quad (2)$$

$$\text{opening:} \quad \gamma_B^e(F) = \delta_B^e(\epsilon_B^e(F)); \quad (3)$$

$$\text{closing:} \quad \phi_B^e(F) = \epsilon_B^e(\delta_B^e(F)); \quad (4)$$

$$\text{top hat:} \quad TH_B^e(F) = F - \gamma_B^e(F). \quad (5)$$

The basic morphological operations are erosion and dilation. Although commonly used on binary images, this approach can be extended to gray-scale images as well. Dilation, in general, causes objects to dilate or grow in size; erosion causes objects to shrink. The amount and the way that they grow or shrink depend upon the choice of the structuring element B. The opening operation is somewhat like erosion in that it tends to remove some of the foreground (bright) pixels from the edges of regions of foreground pixels. However, it is less destructive than erosion in general. As with other morphological operators, the exact operation is determined by a structuring element. The effect of this operator is to preserve foreground regions that have a similar shape to the structuring element, or that can completely contain the structuring element, while eliminating all other regions of foreground pixels. However, "closing" is similar in some ways to dilation in that it tends to enlarge the

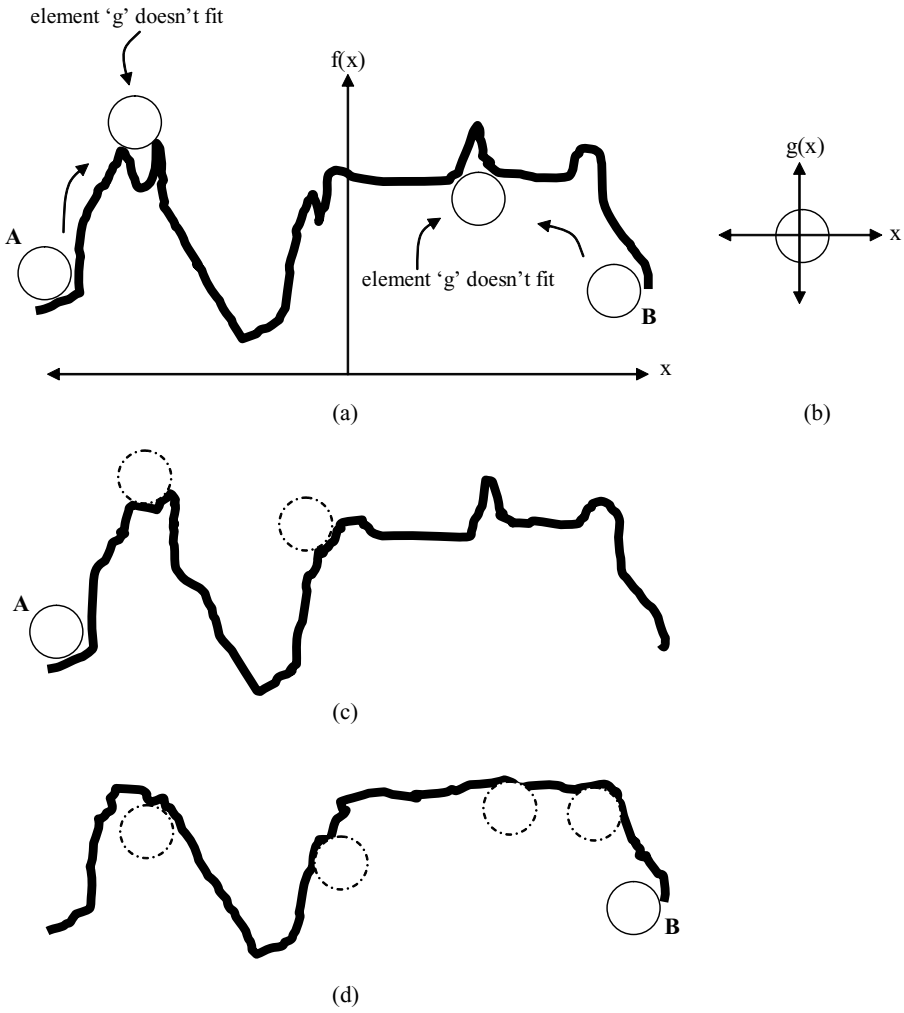

Fig. 3. Illustration of gray-scale opening and closing operation: (a) A gray-scale scan line "$f(x)$"; (b) circular structuring element "$g(x)$"; (c) result of closing showing various locations of structuring element during operation; and (d) result of opening showing various locations of structuring element during operation.

boundaries of foreground (bright) regions in an image (and shrink background color holes in such regions), but it is less destructive of the original boundary shape. The effect of this operator is to preserve background regions that have a similar shape to this structuring element, or that can completely contain the structuring element, while eliminating all other regions of background pixels. Figure 3 shows an example of gray-scale opening and closing operation using a circular structuring element "*g(x)*" on a representative signal "*f(x)*". As seen, when the circular structuring element traces out on top of function "*f*", the regions that cannot fit the element are "closed" (Figure 3c). Similarly, when the circular element traces under function "*f*", the regions that cannot fit in the element are "opened". Morphological reconstruction is most of the time presented using the notion of geodesic distance and hence the term, geodesic operators (Vincent, 1987). They are usually defined with reference to a geodesic distance and type of connectivity. In other words, they depend on a "marker" image F_m (connectivity map) and a geodesic distance d.

The geodesic reconstruction (or opening) is defined by

$$\gamma_{F_m}^{\mathrm{rec}}(F) = sup\big(\triangle_{F_m}^{d}(F)\big),\ d \in I \tag{6}$$

where "*sup*" means supremum of the argument and (*argument*) is the geodesic dilation. Morphological reconstruction processes one image, called the marker, based on the characteristics of another image, called the mask. The high points, or peaks, in the marker image specify where processing begins. The processing continues until the image values stop changing. Morphological reconstruction can be thought of conceptually as repeated

dilations of the marker image until the contour of the marker image fits under the mask image. In this way, the peaks in the marker image "spread out," or dilate. Symbolically, $\phi^{\text{rec}}_{F_m}(F)$ means reconstruction (rec) by closing (ϕ) using the marker image F_m on mask image F and is defined by:

$$\phi^{\text{rec}}_{F_m}(F) = I_{\max} - \gamma^{\text{rec}}_{(I_{\max}-F_m)}(I_{\max} - F) \qquad (7)$$

In this study, we assume that the tree-like geometry of cracks is the only element of our image that is locally uniform and can be described by the following properties:

1. intensity distribution of a cross-section of crack looks like a specific Gaussian curve;
2. they branch like a tree;
3. more or less have a constant width.

The above-listed properties can be further classified into those related to morphological descriptions and those related to the calculation of curvature parameters based on linearity, connectivity, crack width, and Gaussian profile.

4.3 Curvature evaluation

It is possible to study and separate the curvature characteristics of tree-like vascular structures in retinal angiographic images thus using it as a tool to segment vessels for ophthalmic diagnosis (see Zana and Klein 2001 for detailed analysis and mathematical proof). Cracks in pipe scan images, like vessels in retinal angiographic images, also have a tree-like structure and hence can be separated from the rest of the image using their differential properties. *Curvature* in the context of digital images is the curvature in the cross-direction defined for every pixel in the image under the assumption that any nonzero point in the picture has a dominant direction and hence can be considered as part of some crack pattern. Figure 4 schematically explains curvature properties of different elements in a pipe image. There are certain undesirable patterns encountered in the image when extracting cracks that have differential curvature characteristics. They can be classified into different cases that we will refer to in this article.

1. Noise occurring in the data acquisition process, or due to undesirable elements whose texture can be described by a low intensity white noise.
2. Linear features in the background that can be confused with cracks in some parts, but that do not meet all the requirements.
3. Dark thin irregular zones that qualify as nonlinear patterns.

In case 3 (Figure 4b), the image signal appears as thin and irregular linear elements, therefore the curvature takes on positive values on a width smaller than in the case of a crack (see Figure 4a) and it is not necessarily linearly correlated. In case 2 (Figure 4c), the signal tends to be low and disorganized and the curvature will take on positive and negative values in various directions. Thus by setting up a criterion to evaluate the curvature of a neighborhood of pixels in the image, it is possible to detect a group of pixels belonging to the crack feature by the very fact that the curvature will take on positive values over a larger neighborhood (see Figure 4a).

4.4 Crack Detection Algorithm

4.4.1 Contrast enhancement of color images. We implement two simple techniques to achieve better contrast in pipe scan images that lead to better crack detection probabilities.

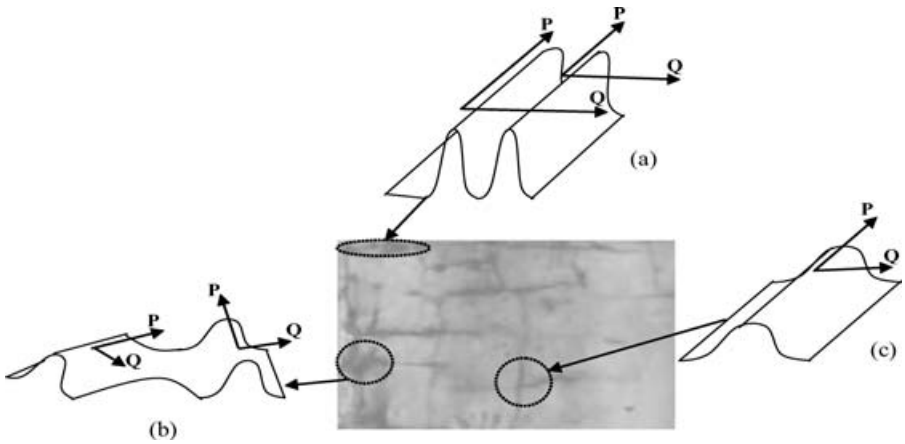

Fig. 4. Curvature profiles of (a) dark thin irregular zones that qualify as nonlinear patterns in the image, (b) linear features in the background that may overlap with cracks. P and Q are the principal directions, and (c) crack.

4.4.1.1 *Method I: Nonlinear quadratic filtering method*

Image enhancement seeks to improve the visual quality of images. However, an inherent difficulty is to define a mathematical criterion for visual quality. As a result, many algorithms remain to a large extent empirical and a final assessment can only be performed by the human observer. In this section, we consider image contrast enhancement based on the unsharp masking method. The common techniques of contrast enhancement generally fall into one of two categories (Gonzalez and Woods, 2002). Techniques belonging to the first category, such as histogram equalization, modify the brightness of each pixel from the statistical information of an image. The techniques in the other category enhance the contrast of images by first separating the high-and/or low-frequency components of images, manipulating them separately and then recombining them together. The unsharp masking or high-frequency emphasis method belongs to this second category. Unsharp masking for edge enhancement, commonly used in the printing industry, is equivalent to adding back the scaled gradient magnitude to the original signal. Mathematically, unsharp masking can be formulated as

$$x_e[m,n] = x[m,n] + \gamma \nabla x[m,n] \tag{8}$$

where $x_e[m,n]$ denotes the enhanced image; $x[m,n]$ represents the original input image; $\nabla x[m,n]$ refers to the gradient of $x[m,n]$ and γ the enhancement factor. "m" and "n" in $x[m,n]$ denote the rows and columns (pixel locations) of the matrix that constitute a 2D image. A discreet Laplacian operator is commonly used as a gradient function (Gonzalez and Woods, 2002). Mitra and Strobel (1995) proposed a modification that is based on replacing the gradient operator $\nabla x[\cdot]$ by an enhancement fraction $\Delta x[m,n]$. This fraction is derived from quadratic filters where

$$\Delta x[m,n] = f\left\{\frac{y[m,n]}{\max(|y[m,n]|)}\right\} \times x[m,n] \tag{9}$$

with $y[m,n]$ denoting the output of the quadratic filter. An example of the quadratic filter is the type 1B quadratic filter defined as (Mitra and Strobel, 1995)

$$\begin{aligned} y[m,n] = {} & 2x^2[m,n] - x[m-1,n+1]x[m+1,n-1] \\ & - x[m-1,n-1]x[m+1,n+1]. \end{aligned} \tag{10}$$

As the filter response $y[m,n]$ in the above equations can take both positive and negative values, the function $\max(\|y[m,n]\|)$ selects the maximum absolute value. The (normalized) quotient $y[m,n]/\max(\|y[m,n]\|)$ is referred to as the *enhancement map*, and the overall product results in an enhancement fraction whose magnitude is bounded by the maximum intensity level of the display device. A quadratic filter derived by Thurnhofer (1994) was considered in the modified algorithm and implemented as shown below:

$$\begin{aligned} & y[m,n] \\ & = 3x^2[m,n] - 0.5 \times (x[m+1,n+1]x[m-1,n-1]) \\ & \quad - 0.5 \times (x[m+1,n-1]x[m-1,n+1]) \\ & \quad - x[m+1,n]x[m-1,n] - x[m,n+1]x[m,n-1]. \end{aligned} \tag{11}$$

This algorithm was applied in a local window within the image for more prominent results. Three sizes of windows used were 3×3, 5×5 and 7×7. The enhancement factor γ was also varied from 0.25 to 1.5 for each window size. A huge database of images with all the parametric combinations yielded 180 images by applying the algorithm on five sample images exhibiting a variety of crack features and patterns and five sample images with different background characteristics. Figure 5 shows one representative original crack color image and the contrast enhanced images using the proposed method. The enhanced images shown are obtained by running a 3×3, 5×5 and 7×7 window and an enhancement factor γ of 0.5. Observations have shown that a 5×5 filter size with an enhancement factor γ of 0.5 gives the best result. Further validation will be possible only when the crack segmentation and detection algorithm is applied to this enhanced image. A high percentage of cracks detected from images that are enhanced using this method will serve as a proof for accepting it to improve image preprocessing.

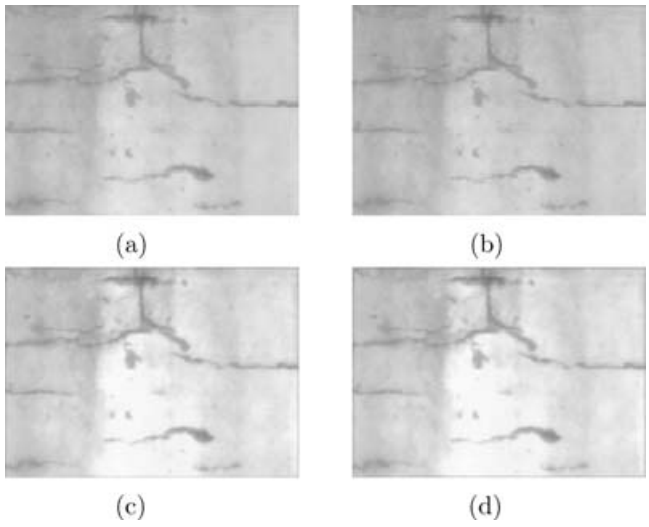

Fig. 5. Nonlinear quadratic filtering method (a) original crack image, (b) 3×3 window, (c) 5×5 window, and (d) 7×7 window enhanced image.

4.4.1.2 Method II: Magnification of dark image features

Crack features are deeper than the pipe surface in a pipe scan image. This causes the deep regions to produce color pixels with lower intensity value compared to the rest of the image. A new approach to enhancement is proposed in this section by increasing the contrast of dark pixels from the estimated "background" image. The output is a gray scale enhanced image. The background image is the image of the pipe without any small features (e.g., cracks). A digital color image is made up of three constituent component images, namely, Red (R), Green (G), and Blue (B) bands. Given the input color image, a median filter is applied to each of the R, G, and B component images. The window size for the median filter is 15 × 15. This was determined based on the width of the crack lines. The window size experimentally selected is large enough to erode the small features and at the same time small enough to be computationally fast. This method picks the dark pixels by comparing the intensity of each pixel in the original color image with that of the background image. The algorithm can be summarized below:

Let M be the original color image of the pipe and let "BackG" be the estimated background image, computed as:

$$\text{BackG} = \text{Median Filter RGB(M)} \tag{12}$$

where Median Filter RGB(M) is a median filter applied to each of the R, G, and B bands of the color image "M". The median filter considers each pixel in the bands in turn and looks at its nearby neighbors to decide whether or not it is representative of its surroundings. Instead of simply replacing the pixel value with the mean of neighboring pixel values, it replaces it with the median of those values. The median is calculated by first sorting all the pixel values from the surrounding neighborhood into numerical order and then replacing the pixel being considered with the middle pixel value. Becauase the median value must actually be the value of one of the pixels in the neighborhood, the median filter does not create new unrealistic pixel values when the filter straddles an edge like feature as applicable in our study. Let GrayM[m, n] be the gray scale value of the color pixel M[m, n] and GrayBackG[m, n] the gray-scale value of color pixel BackG[m, n]. The "enhancement" is described by the following decision function:

$$\begin{aligned} &\textbf{\textit{if}}\ (\text{GrayM}[m,n] < \text{GrayBackG}[m,n]) \\ &\quad \text{Enhanced}[m,n] = \text{GrayM}[m.n] - \text{diff-factor} \\ &\qquad * \| M[m,n] - \text{BackG}[m.n] \| \\ &\textbf{\textit{else}}\ \text{Enhanced}[m,n] = \text{GrayM}[m,n] \end{aligned} \tag{13}$$

where, Enhanced[m, n] is the gray-scale value of the enhanced pixel, diff-factor is the parameter controlling the degree of contrast, and the operator $\|\cdot\|$ is the Euclidean norm.

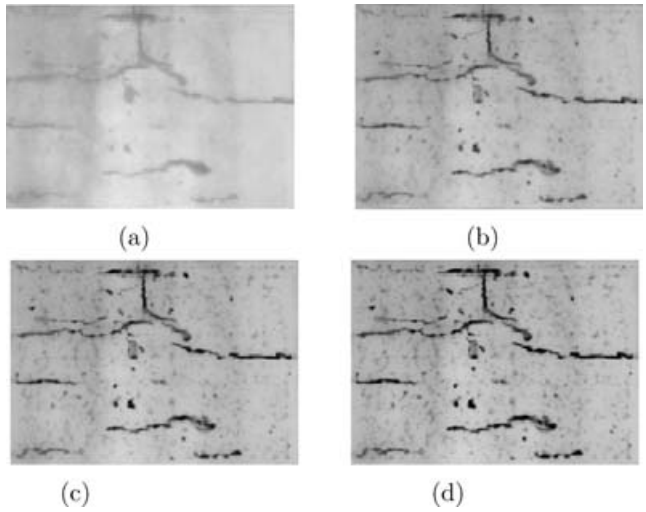

Fig. 6. Magnification of dark features method (a) gray-scale crack image, (b) diff-factor = 2, (c) diff-factor = 3, and (d) diff-factor = 4.

The term ‖M[m, n] − BackG[$m.n$]‖ is the equivalent to the Euclidean distance between the two RGB color vectors M[m, n] and BackG[m, n]. The parameter diff-factor controls the contrast of the dark pixels from the background. Its value should be set large enough to provide sufficient contrast but not too large so as to darken the other gray regions. Figure 6 shows representative images generated by running this algorithm on scanned pipe images from our database similar to the quadratic filter method. Again, suitability of this method as a preprocessing step is subject to the outcome of crack segmentation and the detection phase.

4.4.2 Morphological treatment for the recognition of crack features. We employ morphology-based filters with linear structuring elements taking advantage of the linear property of crack features.

A morphological closing (see Section 4.2) with a linear structuring element will remove a crack or part of it when the element cannot be included in the geometry of the crack. This is true when the structuring element is orthogonally oriented with respect to the crack and is hence longer than the crack width. However, the crack will not be affected when the structural element and the crack have parallel directions. A sum of top hats along possible directions will highlight the cracks irrespective of their inclination in the image if openings along a class of linear structuring elements is performed. But this sum of top hats will recover a lot of noise because the openings require that the structural elements be large enough

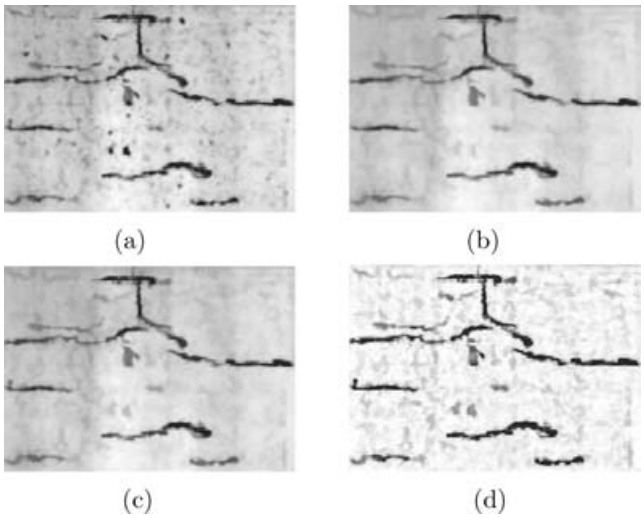

Fig. 7. Steps in the morphology based recognition process: (a) original (contrast-enhanced) image, (b) supremum of closing, (c) geodesic reconstruction, and (d) sum of top hats.

to remove unwanted features in the image that do not fall in the category of cracks. Hence, we perform reconstruction operations using connectivity property of the cracks before taking the sum of top hats (Figure 7).

A geodesic reconstruction of the closed images into the original image $\{F_0\}$ will remove noise while preserving most of the cracks. Mathematically, this operation can be represented as:

$$F_{cl} = \phi_{12}^{rec}\Big(\underset{i=1\cdots 18}{\text{Min}}\{\phi_{B_i}(F_0)\}\Big). \tag{14}$$

Each of the 18 linear (width = 1 pixel) structuring elements B_i is 12 pixels wide and is oriented at every 10° from 0 to 180. The element size is based upon the range of crack widths that are of interest to the municipal authorities. A more detailed discussion on this will follow in Section 5.3. The resulting reconstructed image F_{cl} will not have any isolated round zone whose diameter is less than the size of the structuring element (12 pixels). This step called *linear closing by reconstruction* of size 12 removes noise and other features that do not fit into the geometric definition of cracks. The sum of top hats on the filtered image F_{cl} will enhance all cracks irrespective of their orientations including minor cracks in a low-contrast image. However, the F_{cl} image contains a lot of details corresponding to cases 2 and 3 in Section 4.2.

4.4.3 Final segmentation based on curvature characteristics. It is worthwhile to recall from Section 4.2 that *curvature* is defined as the curvature in the cross-direction which is defined for every pixel under the assumption that any nonzero point in the picture has a dominant direction and hence can be considered as part of some

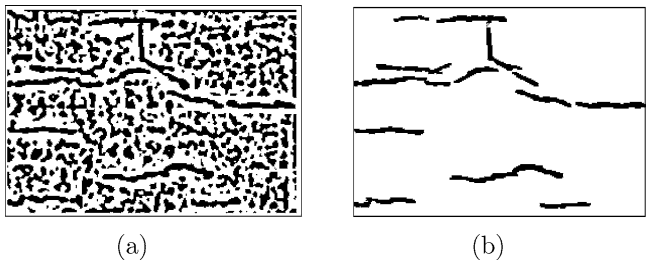

Fig. 8. Laplacian images highlighted around zero (positive values in white and negative values in black): (a) before and (b) after alternating filter.

crack pattern. Its evaluation using the Laplacian operator on a tophats-operated image has been analytically discussed and presented by Zana and Klein (2001). As discussed in Section 4.2, nonlinearly correlated patterns have signals that appear as thin and irregular elements indicating that the curvature gets positive values on a width smaller than in the case of the cracks (see Figure 4). In the case of details like case 2 in Section 4.3, the curvature will have alternating positive and negative values in various directions owing to a low and disorganized signal. This can sometimes lead to represent a curvature trend that fits the crack description. The present study does not attempt to address this issue, which can lead to false detection in a few cases that are rare and have little bearing on the overall performance.

It has been proven that the sign of Laplacian applied to the result image of top hats can be used as a good approximation of the sign of curvature (Zana and Klein, 2001). We compute the Laplacian of F_{cl} to obtain a good estimation of the curvature (see Figure 8a). The final step in the detection process is the application of alternating filters that remove enhanced noise patterns corresponding to cases 2 and 3 as discussed in Section 4.3, thereby producing the final binary crack map. The alternating filtering operation consists of performing a linear closing by reconstruction of size 12, followed by a linear opening by reconstruction of size 12, and finally a linear closing of size 24. These sizes were chosen based on statistics generated on a database of around 225 pipe images acquired from various cities in North America (rationale behind the selection of these values is discussed in Section 5.3).

4.4.4 Steps of the proposed algorithm. We can summarize our algorithm as follows:

Step I: Improve the contrast of RGB pipe image by enhancing the dark pixels from the "background" image.

Step II: Perform crack enhancement described by the following equations in mathematical morphology terms:

$$F_{cl} := \phi^{\text{rec}}_{F_0}\Big(\operatorname*{Min}_{i=1\cdots 18}\{\phi_{B_i}(F_0)\}\Big) \tag{15}$$

$$F_{\text{sum-th}} := \sum_{i=0}^{18}(F_{cl} - \phi_{B_i}(F_0)). \tag{16}$$

The sum of top hats reduces noise and improves the contrast of all linear regions in the image. At this stage, a manual threshold on $F_{\text{sum-th}}$ could result in cracks being segmented out from the image, but in most cases the image would be noisy thus requiring further treatment by curvature evaluation using a Laplacian filter

$$F_{\text{lap}} := \text{Laplacian}\big(\text{Gaussian}^{\text{width=12px}}_{\sigma=2}(F_{\text{sum-th}})\big). \tag{17}$$

Laplacian filters are derivative filters used to find areas of rapid change (edges) in images. Because derivative filters are very sensitive to noise, it is common to smooth the image (e.g., using a Gaussian filter) before applying the Laplacian. This two-step process is called the Laplacian of Gaussian (LoG) operation as shown in the expression above. The Gaussian kernel of 12 pixel width and a standard deviation σ of 2 has been used in this step.

Step III: The third step in the detection process consists of applying a set of filters with linear structuring elements to remove the enhanced noise patterns. The set of alternating filters can be described by

$$F_1 := \phi^{\text{rec}}_{F_{\text{lap}}}\Big(\operatorname*{Min}_{i=1\cdots 18}\{\phi_{B_i}(F_{\text{lap}})\}\Big) \tag{18}$$

$$F_2 := \gamma^{\text{rec}}_{F_1}\Big(\operatorname*{Max}_{i=1\cdots 18}\{\gamma_{B_i}(F_1)\}\Big) \tag{19}$$

$$F_{\text{final}} := \Big(\operatorname*{Min}_{i=1\cdots 18}\{\phi^2_{B_i}(F_2)\} \geq 1\Big). \tag{20}$$

The final closing by a larger structuring element (scaling factor of 2) removes smaller and tortuous segments of cracks that are shorter than the structure element. Cracks are readily identified as pixels whose values are larger than a small positive value such as 1(see Figure 8).

5 DISCUSSION ON THE ROBUSTNESS AND ACCURACY OF THE PROPOSED ALGORITHM

5.1 Pipe image database

The algorithm has been adapted to other types of pipe images: background variations, crack patterns, and color variations based upon the geographical location and condition of the pipe.

Background variations are a result of changing illumination and maintenance conditions for a given pipeline, whereas color variations depend upon the material used for the pipeline, namely, clay, concrete, poly vinyl chloride (PVC), and high-density polyethylene (HDPE). Development of vegetation or algae can also add to the background color patterns. In such images, cracks are less contrasted than in images where the background is generally linear. Careful observation reveals that the crack patterns in pipe scan images indicate a certain extent of damage in that section of pipe. Usually, the probability that there is no crack in a section of pipe is very high as compared to the presence of a crack. Thus, any robust crack recognition and segmentation algorithm should be able to handle images that may or may not contain cracks or defects. In such cases, a good segmentation methodology will not detect cracks where there are none, ultimately saving valuable rehabilitation costs for the authority.

5.2 Evaluation of the proposed algorithm

It is necessary to evaluate the performance of our algorithm on images with varying crack pattern, color, and background, as the case may be, in the field.

The evaluation is carried out by comparing automatically detected cracks with manually plotted cracks (ground truth). A set of connected pixels belonging to the cracks is manually extracted using an in-house graphical user interface (GUI) to replicate the process carried out by a pipe inspector in the field. We use the "buffer-method" (Wiedemann, 1987) for performance evaluation by matching the automatically extracted crack pixels to the reference map or ground truth image. This method is a simple matching procedure in which a buffer of constant predefined width is constructed around the crack data in two steps. In the first step, a buffer of constant width is constructed around the reference crack data by using a morphological dilation operation of size 5×5 (see Figure 9). The parts of the extracted data within the buffer are considered as matched and are denoted as *true positive* whereas the unmatched extracted data are denoted as *false positive*. In the second step, the matching is performed the other way round by constructing a buffer of the same size around the extracted crack data (see Figure 9) and the part of the reference data lying in the buffer is considered as matched. The unmatched reference data are denoted as *false negative*. Probability of detection is defined as the ratio of detected crack pixels to true crack pixels and the probability of a false alarm is the ratio of false-alarm pixels to noncrack pixels in the image. Figure 9 illustrates the matching procedure to quantitatively determine the probability of detection P_{d} and probability of false alarm P_{fa} (false +ve and −ve).

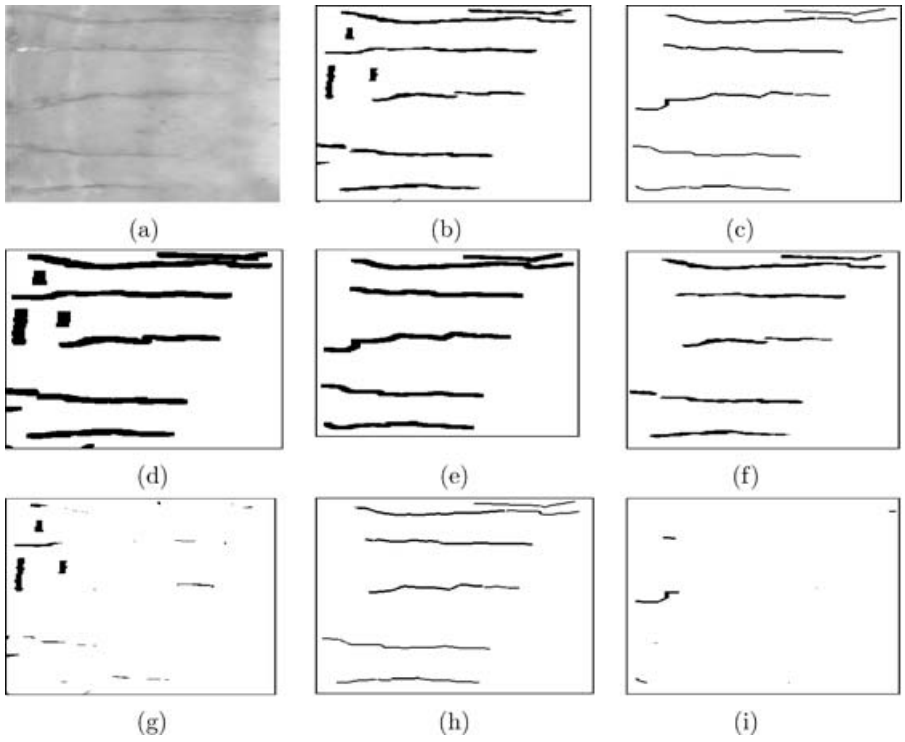

Fig. 9. Matching procedure for detection of true and false pixels. (a) original image, (b) detected cracks, (c) ground truth, (d) and (e) detected and true cracks dilated by a 5×5 structuring element, (f) good points of the filter, (g) falsely detected cracks (false +ve), (h) truly detected cracks and (i) missed cracks (false −ve).

5.3 Selection of algorithm parameters

The size of the structuring element and degree of rotation are two prime parameters that govern the performance of the proposed algorithm. It is imperative to discuss the detection probabilities as a function of these two parameters. Generalization to images of all types can only be effected if the algorithm can perform very well under varying image conditions. Hence, an optimum parameter combination is required that can consistently provide high-detection probabilities under all conditions based on a set criteria for P_{d} and P_{fa} as suggested by the concerned authorities. To quantitatively assess the effect of the structuring element size and degree of rotation on the detection rate, we plot the probability of detection (P_{d}) against the probability of false alarm (P_{fa}) for different structuring element sizes and degree of rotations. We performed experiments on three different classes of pipe images (crack patterns, background, and color) by varying the size of the structuring element ($S = 10$, 12, and 15 pixels) and degree of rotations ($D =$ every 5°, 10°, and 15°) to determine an optimum combination of these two parameters. Given a low false +ve (7%) and false −ve (2%), the corresponding size of structural element and degree of rotation that gives the maximum P_{d} is selected. This is repeated for all the three classes of image and the candidate combination that satisfies the cut-off criteria throughout is finally selected as the generalized optimum parameter combination. Figure 10 shows the probabilities plotted against various parameter combinations for images with varying crack patterns, background, and color. S12-D10 (structural element of size 12 px rotated at every 10°) clearly satisfies the cut-off criteria and is selected as the optimum combination that consistently provides good detection in all types of pipe images.

5.4 Experimental results

This algorithm has been evaluated on a digital database of around 250 images of all types (214 concrete and 36 clay) taken from various cities like Los Angeles, Albuquerque, Toronto, and St. Louis-Missouri in North America. The algorithm was first trained on a training set of 150 images that were not part of the test set. It was found that based on the optimal parameter combination, in most cases, 91% of the cracks were detected. The algorithm missed and/or detected false cracks where there were none amounting to 9% of the total cracks present in the image. All the images were acquired and unwrapped using the SSET camera and its propriety

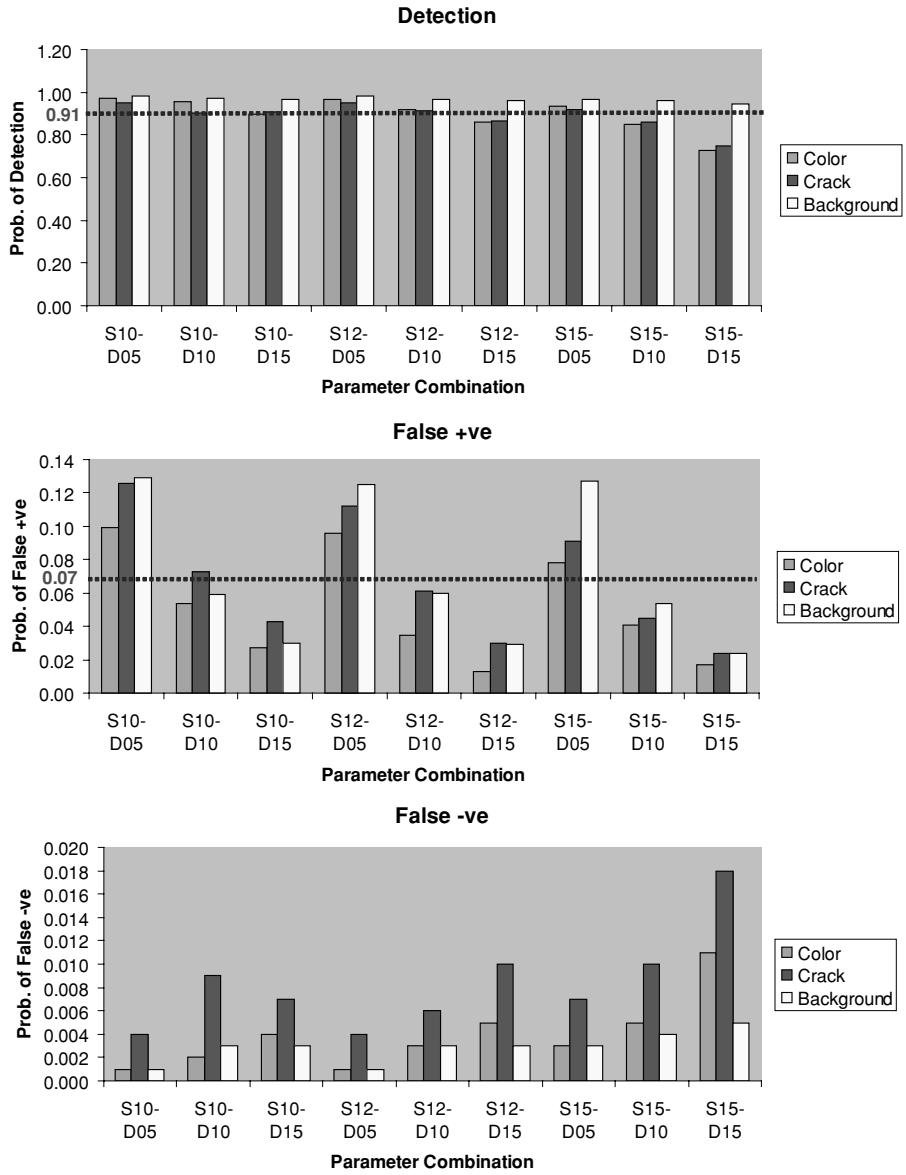

Fig. 10. Bar chart of probabilities for different parameter combinations. Parameter combination S12-D10 consistently meets criteria for P_d, P_{f+ve} and P_{f-ve} in all three image classes. Dotted lines indicate thresholds placed on P_d (91%), P_{f+ve} (7%), and P_{f-ve} (2%, not shown).

software available with the system (Technical Report (SSET), 2001). The typical image size was 285 × 185 × 3 (R, G, and B bands each having 285 rows and 185 columns), however, the database also included images as big as 900 × 550 × 3. The *magnification of dark image features* approach for contrast enhancement was finally selected based on experiments conducted on images from the database after application of the above proposed crack detection algorithm. It was found that the probability of crack detection P_{d} using the nonlinear quadratic filtering method of contrast enhancement was lower than the other method. Robustness was evaluated on noisy images with respect to changing crack patterns (Figure 11), background features (Figure 12), and color (Figure 13). Forty percent of the images (90) that did not have any cracks present produced a perfect image without any detected cracks every single time the algorithm ran with the generalized optimal parameter combination.

There has been false detection in the following cases:

1. extension of crack into a small rounded zone (patch) maintaining the same direction and geometry;
2. cracks are too close to each other;

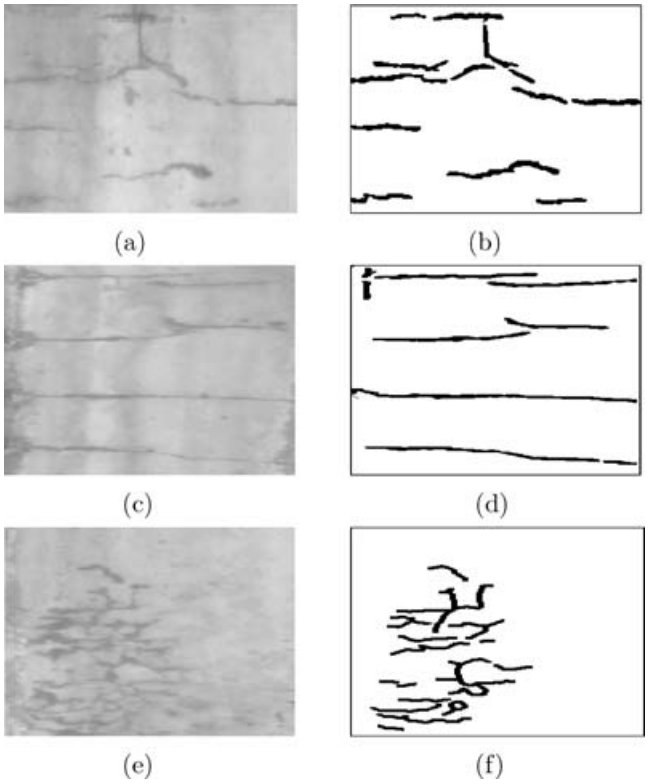

Fig. 11. Image with different crack patterns. (a), (c), and (e)—original color image with multiple, straight and mushroom cracks. (b), (d), and (f)—segmented binary crack map.

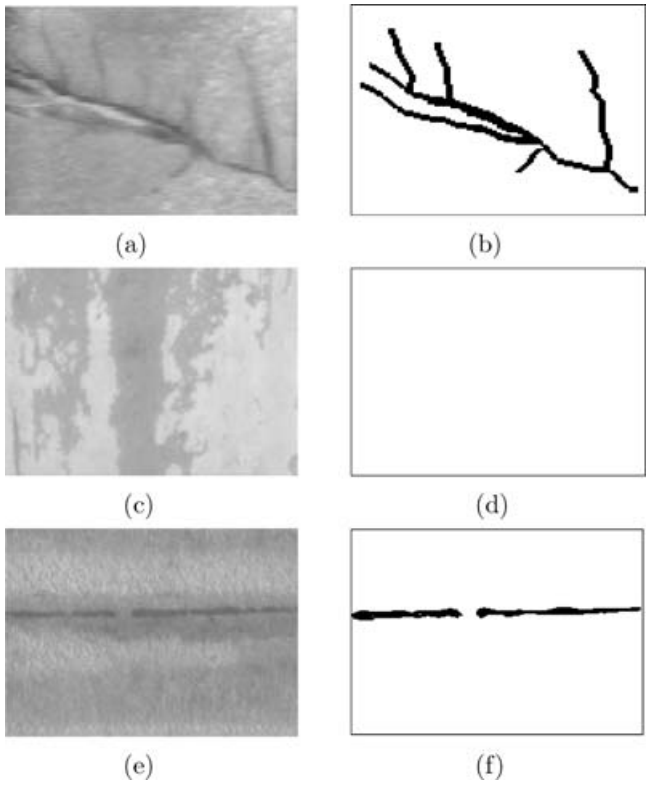

Fig. 12. Image with different background patterns. (a), (c), and (e)—original color image with rough, patchy and smooth background. (b), (d), and (f)—segmented binary crack maps. Note that (c)–(d) pair does not have any cracks present.

3. dark linear structures mistaken for cracks that appear as isolated objects in the image;
4. uniform noise that would modify the connectivity of crack structure thereby disturbing the reconstruction filter and misleading curvature evaluation.

Parts of the crack were not detected mostly in very low contrast (Figure 13) and sometimes in images that had shadows due to illumination issues in the pipe. However, the detection in every case was in accordance with the discussion given in Section 5. This algorithm works on detecting patterns with Gaussian profile bounded at the inflection point. The Gaussian filter applied before the computation of the Laplacian modifies the surrounding texture leading to a shift in location of the inflection point. As a consequence, our experiments show that small cracks appear wider than their real size (see Figure 11). However, this is not a matter of major concern as detection is based on matching the extraction with respect to a buffer width as discussed in Section 5.1.2.

5.5 Comparison of proposed algorithm with other methods

Quantitative performance evaluation is necessary to compare results from different crack detection techniques in addition to an absolute evaluation of extraction and matching results as discussed in Section 5.2. We apply several detection filters to an original image including our proposed algorithm to study the performance with respect to other conventional filters used in the underground pipeline infrastructure industry. We have used Canny's edge detector and Otsu's thresholding technique to extract crack features (Canny, 1986; Otsu, 1979). Figures 13, 14, and 15 show qualitative results from the application of our proposed approach, Canny's edge detection method, and Otsu's thresholding technique to a sample image from all three classes (color, background, and varying crack patterns).The quantification scheme is defined as:

1. Detection Precision

$$D_p = \frac{\text{length of truly detected cracks}}{\text{length of actual cracks}}$$

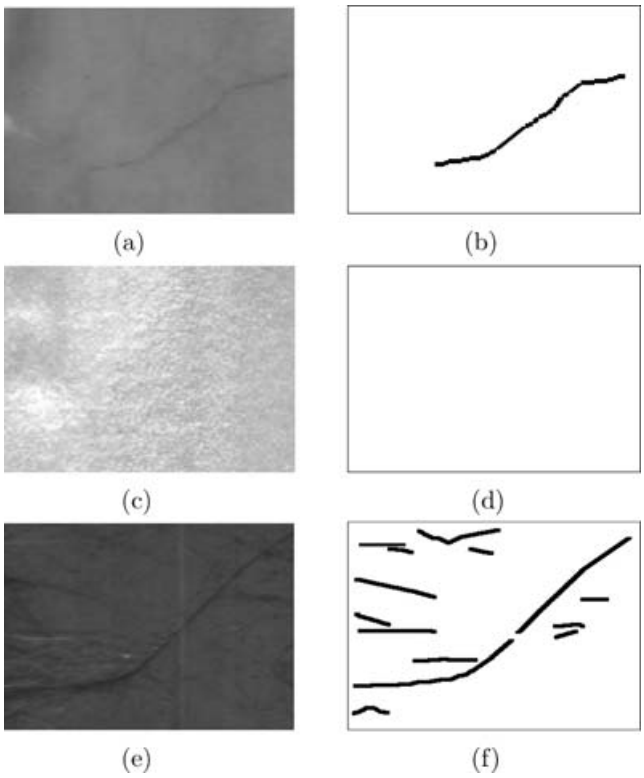

Fig. 13. Image with different color variations.

Detection precision is the percentage of actual cracks that are represented by the detected cracks, that is, the percentage of true cracks that could be extracted by the filters within the buffer width around the extracted data. $D_p \in [0;1]$ and its optimum value is 1.

2. Detection Accuracy

$$D_a = \frac{\text{length of good points of filter}}{\text{length of extracted data}}$$

Detection accuracy represents the percentage of correctly extracted crack pixels, that is, the percentage of extraction that matches the reference crack within the buffer around the reference cracks. $D_a \in [0; 1]$ and its optimum value is 1.

3. Redundant Detection

$$R_d = \frac{\#\text{matched pixels of extr.} - \#\text{matched pixels of ref.}}{\text{no. of pixels of extraction}}$$

The *Redundant detection* represents the percentage to which the correct (matched) crack pixels are redundant, that is, it overlaps itself; $R_d \in]-\infty;1]$ and its optimum value is 0.

The Canny edge detector produces parallel edges (Figures 14, 15, and 16c) suggesting that the largest cracks

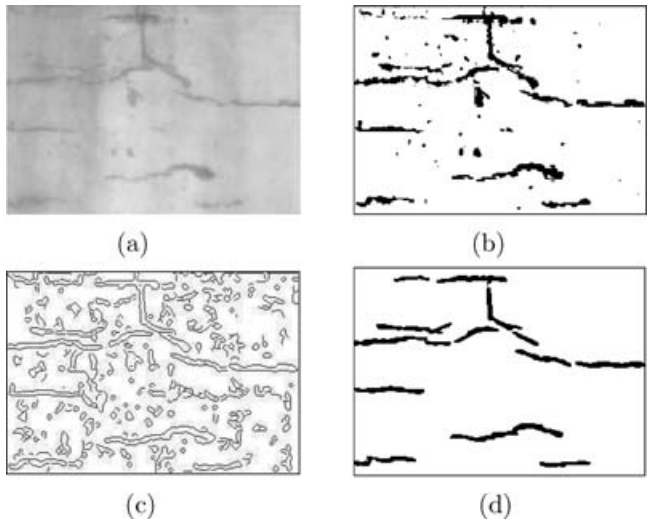

Fig. 14. Edge detection algorithms on crack pattern image: (a) original image, (b) Otsu's thresholding, (c) Canny's edge detector, and (d) proposed approach.

are easily picked up by the detector at the cost of smaller cracks that appear less contrasted. Otsu's thresholding technique selects a threshold based on integration (a global property) of the gray-level histogram. Hence, in areas where the cracks and background path run into each other or low contrast dark images, false detection is inevitable as seen in Figures 14, and 16b. It can be observed that the proposed method produces a binary image that achieves a very small proportion of false

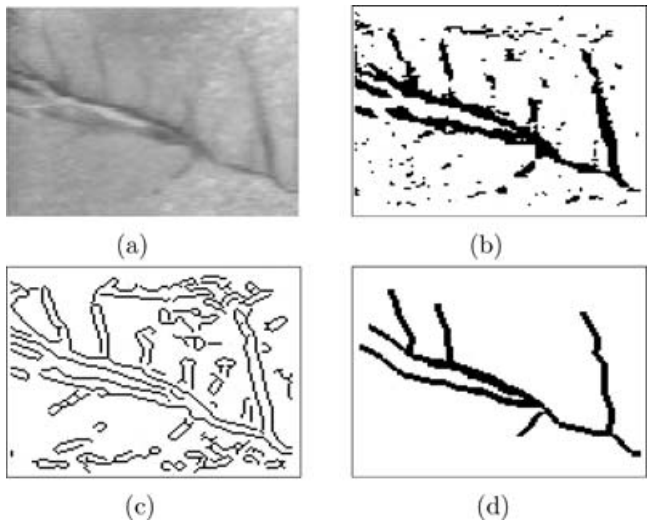

Fig. 15. Edge detection algorithms on background pattern image: (a) original image, (b) Otsu's thresholding, (c) Canny's edge detector, and (d) proposed approach.

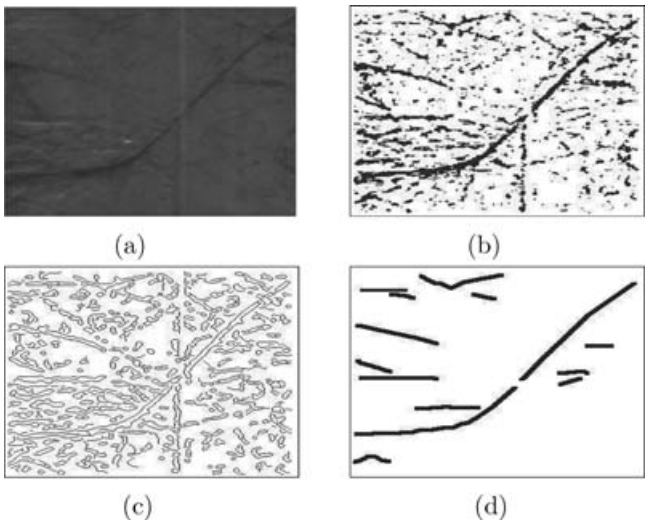

Fig. 16. Edge detection algorithms on color variation image: (a) original image, (b) Otsu's thresholding, (c) Canny's edge detector, and (d) proposed approach.

detection and performs better than Canny's and Otsu's techniques. Images in Figures 13 and 14a that show minor and major cracks are part of sewer pipeline systems in Boston and Los Angeles, respectively. The crack detection step performs quite well detecting most of the crack structures in the image, while missing only some micro-cracks in the images. These cracks might have been present at the time of manufacturing of the pipe and are not a threat to the structural integrity according to industry experts. The image in Figure 15a belongs to a sewer pipeline system in St. Louis, Missouri, and has a dark pipe surface (clay pipe) with a major crack camouflaged in the background in addition to minor cracks. Although there is little contrast between the background and crack features, the crack detection step performed well only missing some minor cracks. Performance evaluation of minor cracks in complex images (Figure 16a) is not easy because it is difficult even for a trained human operator to identify such minor cracks. The quantitative results are summarized in Tables 1, 2 and 3.

Table 1
Performance measures for quantification of proposed approach

Class	*Cracks*	*Background*	*Color*
Detection precision D_p	0.95	0.88	0.90
Detection accuracy D_a	0.98	0.94	0.91
Redundant detection R_d	0.00	−0.01	0.00

Table 2
Performance measures for quantification of Otsu's thresholding technique

Class	*Cracks*	*Background*	*Color*
Detection precision D_p	0.98	0.61	0.62
Detection accuracy D_a	0.37	0.45	0.08
Redundant detection R_d	0.22	0.23	0.24

Table 3
Performance measures for quantification of canny's edge detector

Class	*Cracks*	*Background*	*Color*
Detection precision D_p	0.92	0.61	0.62
Detection accuracy D_a	0.20	0.44	0.07
Redundant detection R_d	0.15	0.17	0.14

6 CONCLUSIONS

Automated crack detection systems that limit the necessity of human inspection have the potential to lower the life-cycle cost of condition assessment of buried pipes. In this article, we have adapted and implemented an efficient algorithm for detecting crack patterns in pipeline images. This automated method can be divided into three steps, namely, contrast enhancement, morphological treatment and curvature evaluation in the cross-direction and finally the alternating filters that produce the final segmented binary crack map. The proposed evaluation scheme adequately estimates the performance of this algorithm in an absolute way and relative to conventional detection techniques used in the underground pipeline inspection industry. The robustness and weaknesses of the algorithm have been discussed to facilitate its use in a larger scheme for condition assessment of underground pipelines. The scope of this article is focused on improving the segmentation methodology in pipeline images. We plan to use this method as a first step toward crack image registration and feature classification in preparation toward an automated pipe condition assessment tool.

REFERENCES

Canny, J. (1986), A computational approach to edge detection, *IEEE Transactions on Pattern Analysis and Machine Intelligence*, **8**, 679–98.

Chae, M. J. & Abraham, D. M. (2001), Neuro-fuzzy approaches for sanitary sewer pipeline conditional assessment, *ASCE J. of Computers in Civil Engineering*, **15**(1), 4–14.

Cheng, H. D. & Miyogim, M. (1998), Novel system for automatic pavement distress detection, *Journal of Computing in Civil Engineering*, **12**(3), 145–52.

Duran, O., Althoefer, K. & Seneviratne, L. D. (2002), State of the art in sensor technologies for sewer inspection, *IEEE Sensors Journal*, **2**(2), 73–81.

Fieguth, P. W. & Sinha, S. K. (1999), Automated analysis and dectection of cracks in underground pipes, in *Proceedings of the International Conference on Image Processing (ICIP)*, 395–99.

Geman, D. & Jedynak, B. (1996), An active testing model for tracking roads in satellite images, *IEEE Transactions on Pattern Analysis and Machine Intelligence*, **18**, 1–14.

Gharpuray, D. & Haas, C. (1993), A Comparison of multisensing methods for the detection of cracks in pavement surfaces, *Pacific Rim Transtech Conference*, **7**, 425–29.

Gokhale, S. R., Abraham, D. M. & Iseley, T. (1997), Intelligent sewer condition evaluation technologies - An analysis of three promising options, *North American NO-DIG 1997 Conference*, North American Society for Trenchless Technology, 253–65.

Gonzalez, R. C. & Woods, R. E. (2002), *Digital Image Processing*, 2nd edn. Pearson Education, Singapore.

Haas, C., Kim, Y., & Greer, R. (1998), A model for imaging assisted automation of infrastructure maintenance, *ASCE Conference on Imaging Technologies Techniques and Applications in Civil Engineering Systems*, **7**(2), 108–17.

Hellwich, O., Mayer, H. & Winkler, G. (1992), Detection of lines in synthetic aperture radar (SAR) scenes, in *Proceedings of the International Archives Photogrammetry Remote Sensing (ISPRS)*, **31**, 312–20.

Iseley, T. (1999), Development of a new sewer scanning technology, *No-Dig America*, North American Society for Trenchless Technology.

Kass, M., Witkin, A. & Terzopoulos, D. (1988), Snakes: Active contour models, *International Journal of Computer Vision*, **1**(4), 321–31.

Maragos, P. & Schafer, R. W. (1990), Morphological systems for multidimensional signal processing, in *Proceedings of IEEE*, **78**(4), 690–710.

Merlet, N. & Zerubia, J. (1996), New prospects in line detection by dynamic programming, *IEEE Transactions on Pattern Analysis and Machine Intelligence*, **8**, 426–31.

Mitra, S. K. & Strobel, N. (1995), Quadratic filters for image contrast enhancement, in *Proceedings of the 20th Asilomar Conference on Signals, Systems and Computers*, **1**, 208–12.

Mohajeri, M. H. & Manning, P. J. (1991), ARIA: An operating system of pavement distress diagnosis by image processing, *Transactions of the Research Record*, **1311**, 120–30.

Morici, P. (1997), Small cameras: Diagnosing sewer laterals quickly and easily, *Trenchless Technology*, **6**(10), 40–45.

Otsu, N. (1979), A threshold selection method from gray-scale histogram, *IEEE Transactions of the System, Man and Cybernetics*, **9**(1), 62–66.

Serra, J. (1982), *Image Analysis and Mathematical Morphology*, Academic Press, London, U.K.

Sharpe, R., Gilbert, J. & Oakes, S. (1995), Expert systems and artificial intelligence applications in engineering design and inspection, *8th International Conference on Industry & Engineering Applications of AI & Expert System, International Society of Applied Intelligence (ISAI)*, 99–109.

Sinha, S. K. & Fieguth, P. W. (2001), Assessment, rehabilitation and maintenance of buried pipes, in *Proceedings of the, ASCE International Pipeline Conference, San Diego, California*.

Sinha, S. K., Karray, F. & Fieguth, P. W. (1999), Underground pipe crack detection using image analysis and neuro-fuzzy algorithm, in *Proceedings, 1999 IEEE International Conference on Intelligent Control/Intelligent Systems and Semiotics, North American Society for Trenchless Technology*, 399–404.

Sinha, S. K., Karray, F. & Fieguth, P. W. (2000), Automated segmentation of underground pipe scanned images, in *Proceedings of the World Automation Congress*, **3**, 161–71.

Sinha, S. K. & Knight, M. (2001), Development of an automated pipeline inspection system, in *Proceedings of the International Conference on Underground Infrastructure, Research,Kitchener, Ontario, Canada*.

Skingley, J. & Rye, A. J. (1987), The Hough transform applied to images for thin line detection, *Pattern Recognition Letters*, **6**, 61–67.

Technical Report (SSET) (2001), *Evaluation of SSET: The Sewer Scanner and Evaluation Technology*. Available at http://www.cerf.org.

Technical Report (WIN) (2001), *Water Infrastructure Network (WIN) Agency Report*.

Technical Report (WIN) (2002), *Water Infrastructure Network (WIN) Agency Report*.

Thurnhofer, S. (1994), Quadratic volterra filters for edge enhancement and their applications in image processing, Ph.D. thesis, University of California, Santa Barbara.

Vincent, L. (1987), Morphological grayscale reconstruction in image analysis: Applications and efficient algorithms, *IEEE Transactions on Image Processing*, **2**(2), 176–201.

Walker, R. S. & Harris, R. L. (1991), Noncontact pavement crack detection systems, *Transactions on Research Record*, **1311**, 149–57.

Wiedemann, C. (1987), External evaluation of road networks, *ISPRS Archives*, **34**(3/W8), 93–98.

Zana, F. & Klein, J. C. (2001), Segmentation of vessel-like patterns using mathematical morphology and curvature evaluation, *IEEE Transactions on Image Processing*, **10**(7), 1010–19.